

# Compact, Fast Blinking Cd-Free Quantum Dots for Super-Resolution Fluorescence Imaging

Anh T. Nguyen, Dustin R. Baucom, Yong Wang, and Colin D. Heyes\*

Cite This: *Chem. Biomed. Imaging* 2023, 1, 251–259

Read Online

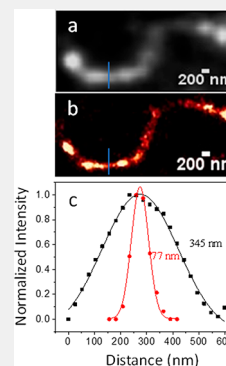
ACCESS |

Metrics & More

Article Recommendations

**ABSTRACT:** Quantum dots (QDs) can be used as fluorescent probes in single molecule localization microscopy to achieve subdiffraction limit resolution (super-resolution fluorescence imaging). However, the toxicity of Cd in the prototypical CdSe-based QDs can limit their use in biological applications. Furthermore, commercial CdSe QDs are usually modified with relatively thick shells of both inorganic and organic materials to render them in the 10–20 nm size range, which is relatively large for biological labels. In this report, we present compact (4–6 nm) CuInS<sub>2</sub>/ZnS (CIS/ZnS) and compare them to commercially sourced CdSe/ZnS QDs for their blinking behavior, localization precision and super-resolution imaging. Although commercial CdSe/ZnS QDs are brighter than the more compact Cd-free CIS/ZnS QD, both give comparable results of 4.5–5.0-fold improvement in imaging resolution over conventional TIRF imaging of actin filaments. This likely results from the fact that CIS/ZnS QDs show very short on-times and long off times which leads to less overlap in the point spread functions of emitting CIS/ZnS QD labels on the actin filaments at the same labeling density. These results demonstrate that CIS/ZnS QDs are an excellent candidate to complement and perhaps even replace the larger and more toxic CdSe-based QDs for robust single-molecule super-resolution imaging.

**KEYWORDS:** copper indium sulfide, zinc sulfide, single molecule, localization microscopy, actin filaments, streptavidin–biotin



## INTRODUCTION

The Abbé diffraction limit leads to conventional imaging having a spatial resolution of approximately half of the photon wavelength which, for visible light, is approximately 200–350 nm. Over recent years, a number of super resolution imaging techniques have been developed to achieve subdiffraction-limited imaging resolution, so-called super-resolution imaging.<sup>1,2</sup> These fall into two general categories of (i) patterned illumination microscopy such as stimulated emission depletion (STED)<sup>3,4</sup> and structured illumination microscopy (SIM),<sup>5,6</sup> as well as the two-objective based 4Pi<sup>7–9</sup> and I<sup>5</sup> M<sup>10,11</sup> microscopies or (ii) single molecule localization microscopy (SMLM) such as photoactivated localization microscopy (PALM),<sup>12</sup> stochastic optical reconstruction microscopy (STORM),<sup>13</sup> points accumulation for imaging in nanoscale topography (PAINT),<sup>14</sup> or stochastic optical fluorescence imaging (SOFI).<sup>15,16</sup>

Patterned illumination microscopies require more complex hardware setups than a typical fluorescence microscope, while the essential principle of SMLM imaging technique relies on mathematical fitting of the fluorescence from a single molecule using a conventional microscope setup,<sup>6,17</sup> and is thus more commonly employed. SMLM is achieved by labeling structures with a high density of fluorescent probes that alternate between bright and dark states. This results in only a small fraction of fluorophores being “on” in a given time frame so that each of the active fluorophores in the frame are separated

from each other by more than the full width at half-maximum (fwhm) of their point spread function, allowing their centroid positions to be precisely localized, usually to within a few nm. A final super-resolution image is reconstructed by assembling the position of each fluorophore over hundreds to thousands of imaging frames to produce a single static image. Thus, progress in SMLM is accomplished by improving the fluorophore rather than the imaging hardware.

The most common fluorophores for SMLM are switchable fluorescent proteins and dyes. However, inorganic quantum dots (QDs) have also been shown to be a suitable candidate, due to their high brightness combined with their natural blinking phenomenon.<sup>18,19</sup> QD blinking-based super-resolution imaging was first reported in 2005, which used Independent Component Analysis (ICA) to accurately localize two-point fluorophores as a function of their separation.<sup>20</sup> Blinking CdSe QDs have particularly been used to improve spatial resolution with super resolution optical fluctuation imaging (SOFI).<sup>15</sup> Wang et al. introduced quantum dot blinking with a three-dimensional imaging (QDB3) technique,

**Received:** January 24, 2023

**Revised:** March 20, 2023

**Accepted:** March 21, 2023

**Published:** April 3, 2023



in which 3D super-resolution imaging with blinking QDs is achieved through extracting the point-spread function (PSF) of individual QDs by subtracting subsequent frames.<sup>21</sup> Multicolor imaging has also been presented using QDs as probes, since their wide excitation spectra allows for a single laser to excite multiple QDs simultaneously.<sup>22–24</sup>

The prototypical Cd-based QDs have issues in bioimaging applications due to their highly toxic cadmium content. Moreover, commercialized Cd-based QDs are usually coated with thick shells and polymeric coatings, which render them up to 15–20 nm in size. These coatings, while providing both improved brightness and chemical stability, tend to also reduce blinking so that the QDs spend most of the time at the on state and rather short time in the off state, which is preferable for most bioimaging applications. However, for SMLM, it is ideal for the off-time of each fluorescent probe to be much longer than the on-time to limit the number of fluorophores that are in the on state within a single imaging frame. To address the problem of lower-blinking QDs, blueing of CdSe/ZnSe QD was exploited in super resolution imaging for microtubules<sup>25</sup> as was the use of two-color QSTORM imaging of microtubules and mitochondria using two sizes of the QDs (QD 705 nm and QD 565 nm).<sup>22</sup> Recently, biocompatible carbon dots were introduced with burst like fluorescent for SMLM imaging of microtubule networks<sup>26</sup> and fixed trout epithelial gill cells.<sup>27</sup> While, carbon dots do not contain toxic elements and are thus preferable to Cd-based QDs, they are often synthesized by refluxing in 6 M HNO<sub>3</sub> followed by two stage ultrafiltration to extract the nanoparticles from the reaction mixture, which are not ideal synthesis conditions.

In this report, we extend the toolbox to low toxicity, fast-blinking QDs for SMLM imaging by synthesizing compact CuInS<sub>2</sub>/ZnS QDs. CuInS<sub>2</sub> (CIS) is a I–III–VI<sub>2</sub> semiconductor with a direct band gap of 1.45 eV and does not contain toxic heavy metals.<sup>28–30</sup> It has been shown previously that the cytotoxicity of CIS/ZnS QDs is low. Compared to Cd-containing QDs that have IC<sub>50</sub> values in the nM range, CIS/ZnS QDs can reach IC<sub>50</sub> values the hundreds of μM range.<sup>31</sup> More recent studies have shown that tuning Cu:In stoichiometry can result in negligible cytotoxicity of CIS/ZnS QDs even up to 50 mM.<sup>32</sup>

As reported previously, we are able to control both the photoluminescence quantum yield/brightness and the blinking behavior of CIS QDs by exposing them to different amounts of zinc stearate after synthesis of the CuInS<sub>2</sub> core, thereby controlling the degree of cation exchange of Cu and In with Zn.<sup>33</sup> In particular, we found that we can synthesize bright QDs with fast blinking by using a limited amount of Zn precursor (0.1 mmol), while increasing the amount of Zn precursor to 4 mmol allows us to increase the fraction of low-blinking QDs from the same batch of CuInS<sub>2</sub> cores. Although the synthesis of these QDs does require high temperatures, no concentrated acids or environmentally dangerous solvents are needed, and the work up only requires simple solvent extraction steps to produce small (<5 nm) QDs with narrow size distributions. We find that these fast-blinking QDs are comparable in resolution for subdiffraction imaging of actin filaments to the brighter but more toxic CdSe QDs and to the previously reported carbon QDs that are synthesized in more dangerous solvents.<sup>26</sup>

## METHODS

### Chemicals

Copper(I) iodide (CuI, 99.999%, Sigma-Aldrich), indium acetate In(Ac)<sub>3</sub>, 99.99%, Alfa Aesar), 1-dodecanethiol (DDT, 98%, Sigma-Aldrich), 1-octadecene (ODE, 90%, Acros), zinc stearate (Zn(St)<sub>2</sub>, Acros), mercaptopropionic acid (MPA, Sigma-Aldrich), 1-ethyl-3-(3-(dimethylamino)propyl)carbodiimide hydrochloride (EDC, ThermoFisher), and NeutrAvidin (ThermoFisher). All solvents were purchased from VWR International. Methanol, hexane, dimethylformamide, and ethyl acetate were of pure grade. All of the water used in this study was ultrapure 18MΩ·cm Millipore water obtained from a Direct-Q 3UV water filtration system.

### Synthesis of CIS QDs

CIS QDs are synthesized by modification of the literature methods.<sup>28,34</sup>

Briefly, 0.292 g of In(Ac)<sub>3</sub>, 0.048 g of CuI, 1 mL of DDT, and 10 mL of ODE were mixed in a 50 mL three-neck round-bottom flask (rbf). This solution was first degassed under vacuum for at least 30 min at room temperature, then purged with argon for 30 min. Subsequently under argon flux the solution was heated to 210 °C for 40 min under argon flow. The color of the solution changed from yellow to orange to deep red as the QDs grew in size. The solution was cooled and then centrifuged at 4000 rpm for 10 min. The precipitate was disposed of, and the solution was used for subsequent exposure to the zinc precursor.

### Synthesis of CIS/ZnS QDs

0.1 mmol (0.063 g) of Zn(St)<sub>2</sub> was added to a 50 mL RBF. Then, 5 mL of ODE, 1 mL of DDT, and 5 mL of CIS QDs were added to the RBF. The mixture was stirred under vacuum at 60 °C for 30 min and backfilled with argon for 30 min. Under argon flux, the reaction temperature was increased to 230 °C. After 6 h, the reaction solution was cooled to room temperature and washed three times with a 50/50 mixture of hexane and methanol. Afterward, the sample was precipitated by adding excess acetone. The flocculent precipitate was centrifuged at 4000 rpm for 10 min and the supernatant decanted.

### Aqueous Phase Transfer of CIS/ZnS

The aqueous phase transfer was achieved by replacing the initial surface ligands, DDT by MPA. A mixture of MPA (2 mL, ~20 mmol) and 100 mg of dried CIS/ZnS QDs were added into 3 mL *N,N*-dimethylformamide (DMF), which formed a turbid solution. Then, the mixture was heated to 130 °C and stirred under argon. After 10–15 min, the mixture solution gradually became clear. Finally, the product was precipitated by adding 10 mL ethyl acetate and centrifuged at 4000 rpm for 5 min. The precipitate was dissolved in basic solution (pH ~ 9) for storage.

### Conjugation of MPA-CIS/ZnS QDs with Neutravidin

Neutravidin was conjugated to the COOH-functionalized CIS/ZnS QDs by a straightforward EDC coupling method. Briefly, in an Eppendorf tube, 10 μL of 16 μM stock solution of MPA-CIS/ZnS was diluted to 50 μL using 10 mM borate buffer, pH 7.4. Then, 200 μL of 10 mg/mL neutravidin was added to the QD solution. Ten mg/mL of EDC stock solution was prepared just before use. Immediately, 50 μL of 10 mg/mL EDC stock solution was added to the mixture of QD and neutravidin. The solution was gently mixed and left at room temperature for 10 min. The solution was transferred to a centrifugal ultrafiltration tube (100 kDa cutoff, Pall Life Sciences) and centrifuged at 6000 rpm for 5 min to remove any excess unbound protein. The QDs were redissolved in PBS buffer (20 mM, pH 7.2), and filtered through a clean centrifugal filter unit (0.2 μm, Pall Life Sciences) to remove aggregates. The purified neutravidin-conjugated CIS/ZnS QD solution was stored at 4 °C until further use.

### Polymerization of Actin

F-actin (or actin filaments) was freshly prepared before each imaging experiment. Biotinylated G-actin monomer was dissolved to 0.2 mg/mL with general actin buffer and keep it on ice. 100 μL ice cold actin polymerization buffer was added and then left overnight at 4 °C to

form actin filaments (F-actin). The solution was then diluted in water to a total volume of 1 mL.

### Sample Chamber Preparation

Microscope slides and coverslips were immersed with aqua regia for 30 min, then rinsed with ultrapure water. Then, slides and coverslips were sonicated, further rinsed with water and then dried with nitrogen gas. Sample chambers were constructed as follows: Two strips of double-sided tape were placed onto the slide along the short edges, leaving a gap of 3–5 mm at the center. A cleaned coverslip was placed on top of the slide/tape under pressure to produce a watertight channel. The open ends of the chamber are left open and served as inlet and outlet, whereby capillary forces allow the channel to be filled via a pipet on one end and a tissue on the other end to wick the solution, thereby allowing the solution in the channel to be easily exchanged. The channel volume is several microliters.

### Morphological Characterization of QDs

Bright field TEM images were taken on a FEI Titan 80-3000 TEM with an accelerating voltage of 300 kV. The average QD size and size distribution were estimated by analyzing TEM images of ~100 QDs using ImageJ.

### Optical Measurements of QDs at the Ensemble Level

Absorption spectra of CIS/ZnS QDs before and after aqueous transfer were obtained by a Hitachi U-3900H UV/vis-spectrophotometer and fluorescence emission spectra were recorded with a PerkinElmer LS55 Luminescence Spectrometer. The relative PL quantum yields (QYs) of various QD samples were comparatively studied by comparison with that of Rhodamine 6G (95% in ethanol) as follows:

$$QY_{\text{QD}} = QY_{\text{R6G}} \times (\text{OD}_{\text{R6G}}/\text{OD}_{\text{QD}}) \times (n_{\text{QD}}/n_{\text{R6G}})^2$$

where  $n_{\text{QD}}$  is the reflective index of hexane for DDT-CIS/ZnS and water for MPA-CIS/ZnS and  $n_{\text{R6G}}$  is the reflective index of ethanol.

The excitation wavelength was set at 485 nm and the optical density (OD) used was ~0.05.

### Fluorescence Imaging and Single Molecule Analysis

All single molecule/particle imaging on coverslips were performed on an Olympus IX 71 inverted fluorescence microscope (Olympus Optical Co., Japan) in total internal reflection fluorescence (TIRF) mode. The QDs were excited using a 488 nm laser (Dream Lasers Technology Co. Ltd., Shanghai, China), and the laser power monitored in front of an oil-immersion microscope objective (NA1.45/100×, Olympus Optical Co., Japan) was measured to be 5 mW. The laser was focused onto the back plane of the objective to provide an illumination area of ~200 × 200 μm<sup>2</sup>. Fluorescence from the sample was collected by the same objective, separated from the excitation light by a dichroic mirror and emission filters (632/148, Semrock), and then directed into an electron-multiplying charge coupled device (EM-CCD, ANDOR iXON Ultra 888) camera. The imaging array was 1024 × 1024 pixels with 13 × 13 μm<sup>2</sup>/pixel. The frame rate was set at 20 fps (50 ms/frame) for all samples utilizing a frame transfer approach in which the next frame is acquired while the previous frame is read out, allowing for continuous movies to be acquired.

### Blinking Statistical Analysis

For DDT-CIS/ZnS, a single particle experiment was prepared by spin-casting freshly diluted QDs in hexane. The QD particle density was controlled by changing the concentration of the QDs in the solution before spin coating. For MPA-QDs, the QDs were immobilized on a coverslip surface by first functionalizing them with neutravidin, as described above. To prepare the sample chamber to immobilize the neutravidin-functionalized QDs, a 20 μL mixture of mPEG-silane and biotinylated mPEG-silane (ratio 99:1) dissolved in water was pipetted into the sample chamber, incubated for 10 min, and rinsed with ~30 μL water. Following this, 20 μL neutravidin conjugated CIS/ZnS QDs were added to the sample chamber, incubated for 10 min, and rinsed with 30 μL water. Movies of blinking QDs were measured and analyzed as previously described<sup>33</sup> to

provide on- and off-time probability densities, as well as to provide average on and off dwell times. Only QDs in the central ~200 × 200 pixels portion of the CCD chip were used to minimize the effects of illumination power variations due to the 2-D Gaussian laser illumination profile. At least 100 dots were randomly selected and analyzed for each sample. All measurements were performed at room temperature.

### Localization Precision

Analysis of the localization precision for a single QD used the blinking movies taken, as described above and processed by either a homemade code, written in Matlab, or by ThunderSTORM,<sup>35</sup> an ImageJ plugin. Briefly, the integrated signal was collected from 7 × 7 pixels around the maximum-intensity center pixel of the PSF. To avoid the crosstalk of multiple particles into an intensity trajectory, any fluorescent spot within five pixels of another fluorescent spot was omitted from analysis.

### Super-Resolution Imaging of QD-Labeled F-Actin

A 20 μL mixture of mPEG-silane and biotinylated mPEG-silane (ratio 99:1) dissolved in water was pipetted into the sample chamber, incubated for 10 min, and rinsed with ~30 μL water. 60 μL neutravidin (10 mg/mL) was added and incubated for 10 min, followed by rinsing with ~100 μL ddH<sub>2</sub>O to remove unbound neutravidin. Twenty μL of biotinylated actin filaments was then added to the sample chamber, followed by rinsing with 40 μL water. Twenty μL neutravidin-conjugated CIS/ZnS QDs or commercial streptavidin-conjugated CdSe/ZnS QDs (QSS600, Ocean Nanotech) was then added to the channel, incubated for 10 min, and rinsed with 40 μL water.

For reconstructing of super resolution images, a time series of fluorescence images were acquired at 100 ms/frame for several minutes. Usually 1–2 min is enough to obtain good super-resolution images. The super-resolution images were then reconstructed with ThunderSTORM.<sup>35</sup> This readily accessible plugin provides a complete tool for image processing, particle localization, and visualization of data.

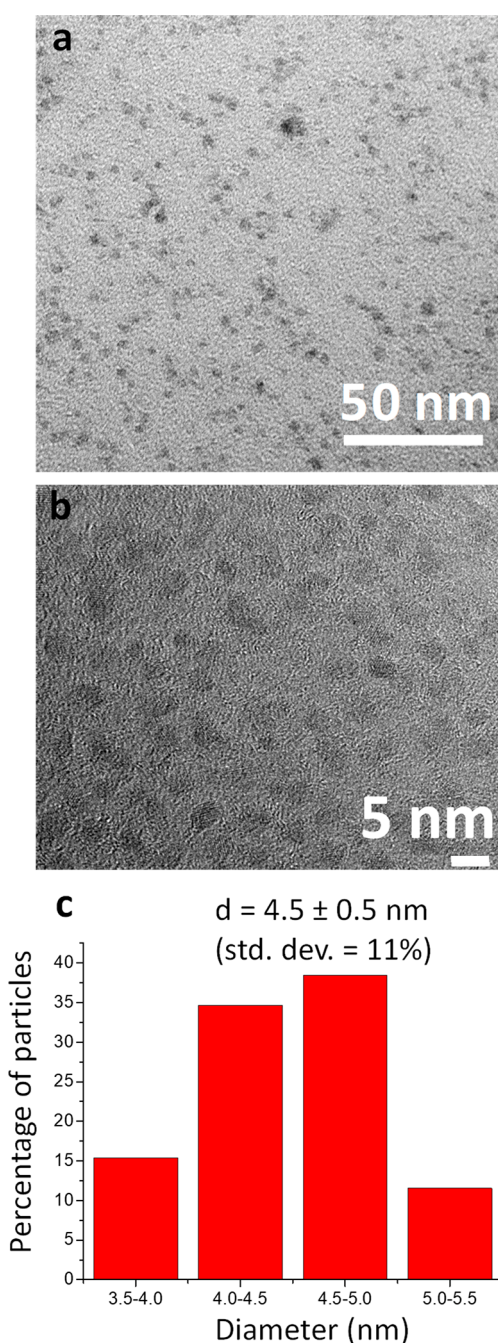
## RESULTS AND DISCUSSION

Figure 1 shows representative TEM images (low resolution and high resolution) and size distribution of the synthesized CIS/ZnS QDs, showing homogeneously spherical particles with an average size of <5 nm and a narrow size distribution of ~0.5 nm. Generally, the smaller the fluorophore size, the more favorable they are for biological imaging applications, especially in spatially confined conditions such as in cell junctions,<sup>36</sup> or in overlapping/interacting biological structures.

One of the major drawbacks of QD fluorophores for biological imaging is that it is difficult to maintain a small size while at the same time improving their optical properties. In addition to their less toxic composition, the small size of these CIS/ZnS QDs are particularly attractive compared to the more typical core/shell based CdSe/ZnS QDs. A key reason that these QDs are able to maintain a relatively small size is that, in the “shelling” step, cation exchange/alloying occurs rather than just addition of a pure shell, which limits size growth while still allowing for improvement of their fluorescence properties.<sup>33</sup>

Figure 2 shows the fluorescence emission spectra and the PL QY of QDs before and after ligand exchange from DDT to MPA, and transfer from hexane to water. A slight red shift is observed, together with a two-fold decrease in PL QY from 60% to 30%. The red-shift and decrease in PL QY upon ligand exchange and water solubilization is consistent with earlier results for CIS/ZnS QDs,<sup>37</sup> and CdSe/ZnS.<sup>38,39</sup>

Figure 3 shows the blinking behavior of CIS/ZnS with the native DDT ligands and after ligand exchange/neutravidin functionalization, compared to commercial streptavidin-



**Figure 1.** Representative (a) low-resolution TEM image and (b) high-resolution TEM of as-synthesized DDT-CIS/ZnS QDs and (c) their size distribution.

functionalized CdSe/ZnS. Representative traces of intensity vs time are shown in Figure 3a–c, and indicates that streptavidin-CdSe/ZnS QDs spend most of the time at the on state, with brief sojourns to the off-state. In contrast, both DDT-CIS/ZnS and neutravidin-CIS/ZnS QDs show burst-like fluorescence, spending most of their time in the off-state.

This is further quantified in the statistical analysis of blinking. The average on and off dwell times are calculated for each type of QD in Figure 3d and 3e, respectively. Both DDT-CIS/ZnS QDs spend an average of  $\sim 0.25$  s in the on state (corresponding to  $\sim 4$  frames at 50 ms per frame), and an average of  $\sim 16.5$  s in the off state ( $\sim 330$  frames). When neutravidin is added to CIS/ZnS QDs, they spend the same

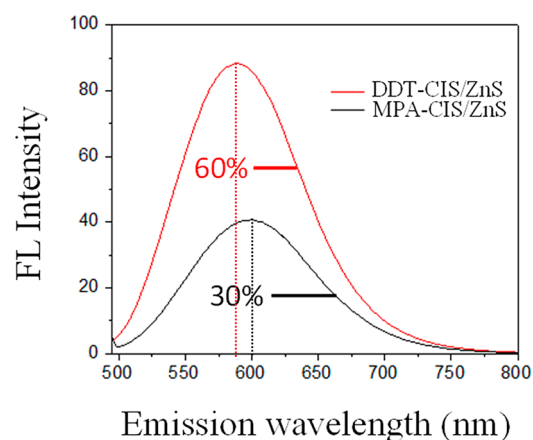


**Figure 2.** PL emission spectra and QY of CIS/ZnS QDs before and after ligand exchange.

$\sim 0.25$  s ( $\sim 5$  frames) in the on state and  $\sim 5.4$  s (108 frames) in the off state. In contrast, CdSe/ZnS QDs spend  $\sim 1.65$  s on average in the on-state ( $\sim 33$  frames), and  $\sim 1.1$  s ( $\sim 22$  frames) in the off state. In other words, CIS/ZnS QDs spend on average between 1.2% and 3.6% (depending if neutravidin is attached or not) of measured frames of a movie in the on state, while CdSe/ZnS spend  $\sim 60\%$  of measured frames in the on state. The number of frames that a QD is on compared to off is an important consideration for super-resolution imaging, and this data suggests that CIS-ZnS QDs should be extremely well-suited for super-resolution imaging.

Figure 3f and 3g shows the probability density of the on dwell times and off dwell times, respectively, for over 100 QDs of each sample. The data is plotted on a log–log scale, highlighting the wide distribution of time scales over which blinking can occur. The data clearly shows that, in line with the average dwell times, the probability density curves for the on-state of streptavidin-CdSe/ZnS QDs are much longer compared to that of DDT-CIS/ZnS and neutravidin-CIS/ZnS QDs. For the probability density distributions of the off state, there is an even more pronounced difference of CdSe/ZnS compared to CIS/ZnS QDs.

Since the first observation of blinking phenomenon in CdSe QDs in 1996,<sup>40</sup> the blinking mechanism has been the focus of a large number of studies, and much progress has been made in both understanding it and controlling it, at least for binary II–VI QDs, such as CdSe-based (see ref 41 and references therein). The most widely accepted explanation is that blinking arises when the photoexcited electrons (or holes) become localized in trap states on the surface of nanocrystals or the surrounding environment.<sup>42</sup> In the resultant charged/trapped nanocrystals, the fluorescence is quenched via nonradiative recombination until the electrons (or holes) return to the nanocrystal emitting core, balancing the charges and rendering it bright again.

However, the exact nature of these trap states, and the mechanisms in which charge carriers are trapped and detrapped is still actively debated in the literature and, therefore, there is still a great deal of discussion as to whether the probability densities for the On-State and the Off-State in QDs are best represented by a power-law distribution, or by a multiexponential distribution.<sup>41,43–46</sup> Since it is not yet clear which function best describes blinking in CIS/ZnS QDs,<sup>47</sup> and an in-depth discussion on the details of the underlying blinking mechanisms of CIS/ZnS is beyond the scope of this study, we

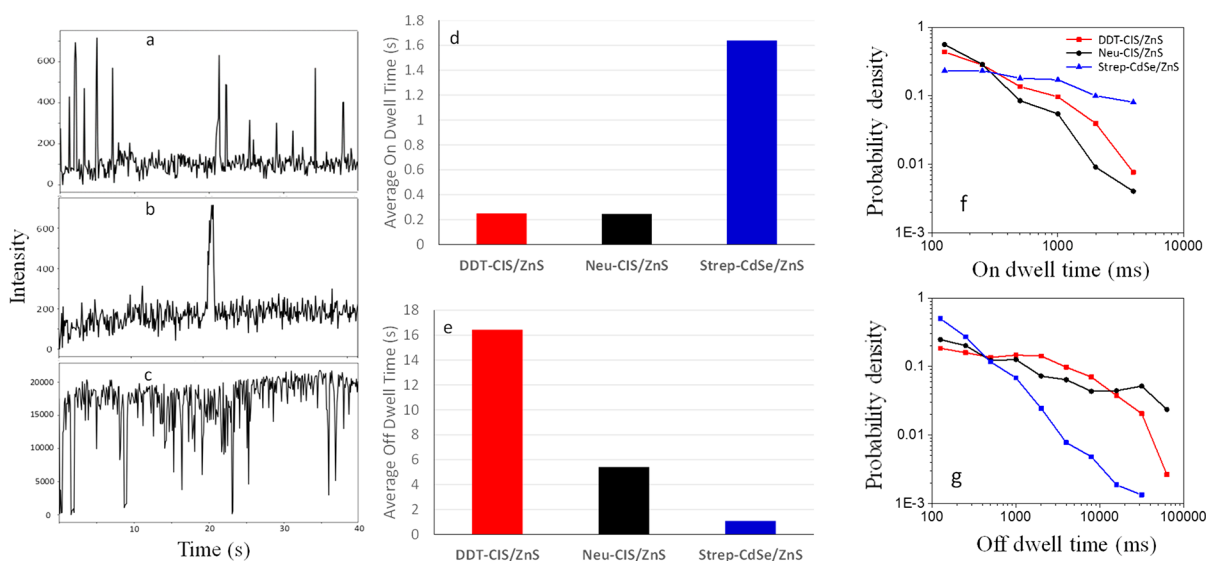


**Figure 3.** Representative traces of intensity vs time of (a) DDT-CIS/ZnS QDs, (b) Neutravidin-CIS/ZnS QDs, and (c) streptavidin CdSe/ZnS under continuous illumination. Statistical analysis for (d) average on dwell times and (e) average off dwell times of over 100 blinking QDs of each type. Probability density distributions for (f) on dwell times and (g) off dwell times of over 100 blinking QDs of each type, shown on log–log scale highlighting the wide range of time scales that blinking events can occur on.

do not specifically fit the probability density curves in Figure 3f and 3g. However, it is clear that rapid switching between on and off states gives blinking QDs great potential for super resolution localization imaging. Furthermore, for fluorescent probes that spend the majority of their time in the off state, while only giving burst-like signals in the on state, a higher density of probes can be labeled on samples to be imaged, resulting in more details for the final reconstructed image.<sup>26</sup> Therefore, as stated above, the blinking data for the CIS/ZnS QDs shown here suggests them to be extremely well suited toward this type of imaging application.

As a first step toward this goal, it is necessary to characterize the localization precision of single QDs. We compare the localization precision of our neutravidin-CIS/ZnS to commercial streptavidin-CdSe/ZnS QDs in Figure 4. The localization precision can be calculated according to eq 1,<sup>48</sup>

$$\sigma^2 = s^2/N + a^2/(12N) + 8\pi s^2 b^2/(N^2 b^2) \quad (1)$$

where  $s$  is the standard deviation (SD) of the PSF,  $a$  is the dimension of a given pixel (130 nm in our setup),  $b$  is the background noise (found by analyzing pixels in the image that contain no QD), and  $N$  is the number of photons collected from the fluorophore (the integrated area of the PSF shown in Figure 4c (CIS) or 4g (CdSe)).

Using these images, we found the average localization precision of the CIS/ZnS QDs to be  $7.2 \pm 1.9$  nm and CdSe/ZnS QDs to be  $1.6 \text{ nm} \pm 0.2$  nm. Clearly, under these idealized conditions, CdSe/ZnS can be localized to a much higher precision, primarily a result of the much higher brightness of commercial CdSe/ZnS QDs. One of the key aims of our lab is to improve the brightness of CIS/ZnS QDs, while still being able to control blinking, but the current localization precision of <10 nm is still comparable to or better than many other fluorophores used for SMLM-based super-resolution imaging.

To evaluate the effectiveness of super-resolution localization in separating QDs that are close to each other, a region of the image in which CIS/ZnS QD emission overlapped was chosen. Figure 5a and 5b shows the conventional TIRF image in which

the maximum intensity of each pixel over 300 frames was determined (a maximum intensity projection image to show the intensity of the QD only when it is on) and the reconstructed super-resolution image, respectively. Figure 5c shows the cross section of the blue line shown in Figure 5a and 5b. For the conventional TIRF image, the PSFs of the two QDs overlap significantly, showing that they are difficult to resolve even close to the Abbe diffraction limit of 350 nm. For the SMLM reconstructed image, the peaks become clearly well resolved. On the basis of the line profiles, this spatial resolution will persist down to the 10s of nm separation.

Actin is one of the key proteins involved in muscle contraction, cell division, and migration. As a monomer, it is a globular protein with molecular weight of 42 kDa and diameter of 5 nm. In the presence of salts and magnesium ions, it polymerizes into long filaments with two helically twisted strands.<sup>49,50</sup> The length of actin filaments can reach up to several microns, while the thickness is about 10 nm (size of two actin monomers), making them an ideal model to test super-resolution imaging of a real biological system.<sup>51,52</sup>

First, to determine if the change in buffer and local environmental conditions affects QD blinking, we labeled f-actin at low density so that single isolated QDs could be analyzed for their blinking behavior, particularly to quantify the average on and off dwell times/frames. This data is shown in Figure 6, which compares the average on and off dwell times of the QDs before (as shown in Figure 3) and after binding to f-actin. The data shows that the both the average on dwell times and average off dwell times becomes smaller for CIS/ZnS when bound to f-actin. The average on dwell time is  $\sim 0.15$  s (3 frames) and the average off dwell time is 3.4 s (68 frames), resulting in CIS/ZnS QDs being on for  $\sim 4.2\%$  of the frames, similar to when they are not bound to f-actin. CdSe spends about the same average time in the on state when they are on f-actin as when they are not on f-actin (1.62s, 32 frames). However, they spend even less time in the off state when they are on f-actin (0.65s, 13 frames) resulting in CdSe/ZnS QDs being on for  $\sim 71\%$  of measured frames, which is even more than when they are not on f-actin.

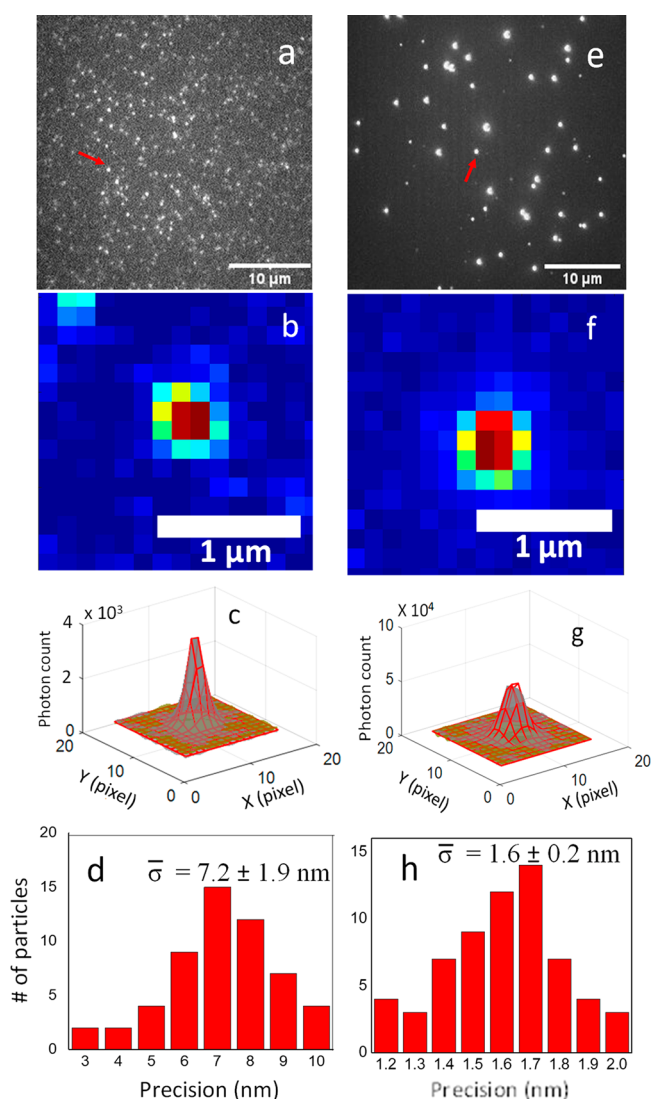


**Figure 4.** Comparison of localization precision for CIS/ZnS and CdSe/ZnS. Wide field fluorescence image of immobilized (a) CIS/ZnS QDs and (e) CdSe/ZnS QDs. Zoomed in false-color image of a single (b) CIS/ZnS QD and (f) CdSe/ZnS QD. 2-D intensity profiles of a single (c) CIS/ZnS QD and (g) CdSe/ZnS QD. Histogram of localization precision found by fitting the 2-D intensity profiles for multiple single (d) CIS/ZnS QD and (h) CdSe/ZnS QD.

Finally, QDs were labeled onto biotinylated f-actin at higher density to provide super-resolution images of f-actin filaments. The top panel of Figure 7 illustrates how QDs were labeled onto f-actin filaments (see Methods Section for details). The width of actin filaments from the Gaussian fit (fwhm) is determined to be 79 nm for CIS/ZnS QDs and 76 nm for CdSe/ZnS, which is approximately 4.5–5 times higher resolution than that acquired by conventional TIRF imaging (361 nm for CIS/ZnS and 379 nm for CdSe/ZnS). This is an interesting result, since the localization precision of CIS/ZnS QDs is 4.5 times lower than that of CdSe/ZnS QDs but result in about the same resolution for SMLM imaging of actin filaments. This can be explained by the fact that even though a single, isolated CdSe/ZnS QDs provides better localization precision due to their higher brightness, their lower blinking means that they mostly stay in the on state. Thus, the PSF of multiple QDs may overlap in a single frame that leads to a less

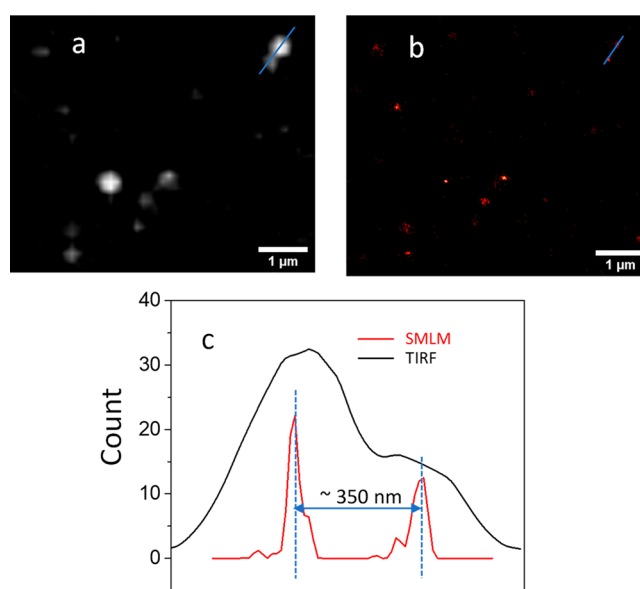


**Figure 5.** (a) Conventional TIRF image and (b) reconstructed (or SMLM) image of immobilized QDs. (c) Line scan profile/cross-section of two closely spaced QDs. The line indicating the cross section is shown in (a) and (b).

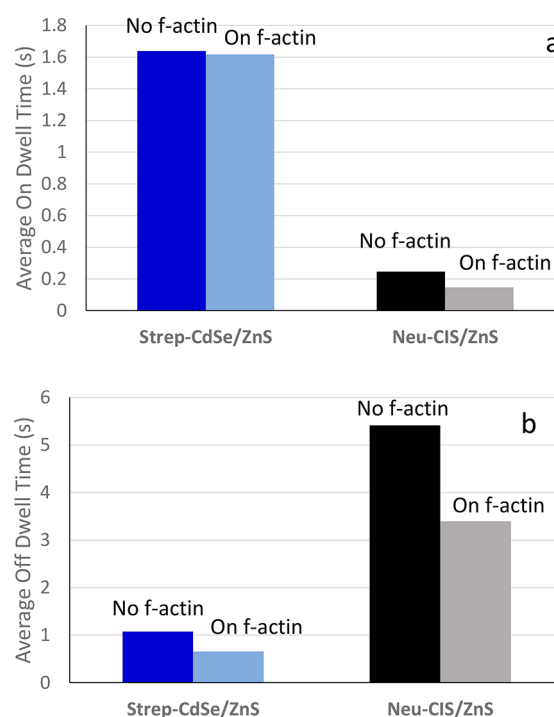


**Figure 6.** (a) Average on dwell time and (b) average off dwell time for Strep-CdSe/ZnS and Neu-CIS/ZnS without f-actin and when added onto f-actin.

precise localization when labeling at a similar density to the faster-blinking, albeit less-bright CIS/ZnS QD. This is in the same range as previously reported for carbon QDs.<sup>26</sup> However, when compared to the ~10 nm expected width of actin filaments, these results still leave room for some improvement for all 3 types of QD (CdSe/ZnS, CIS/ZnS, and carbon QDs). For example, Endesfelder et al. achieved a width of 30 nm in imaging actin filaments when labeling them with both carbocyanine fluorophores Cy5 and Alexa 647 organic dyes.<sup>53</sup>

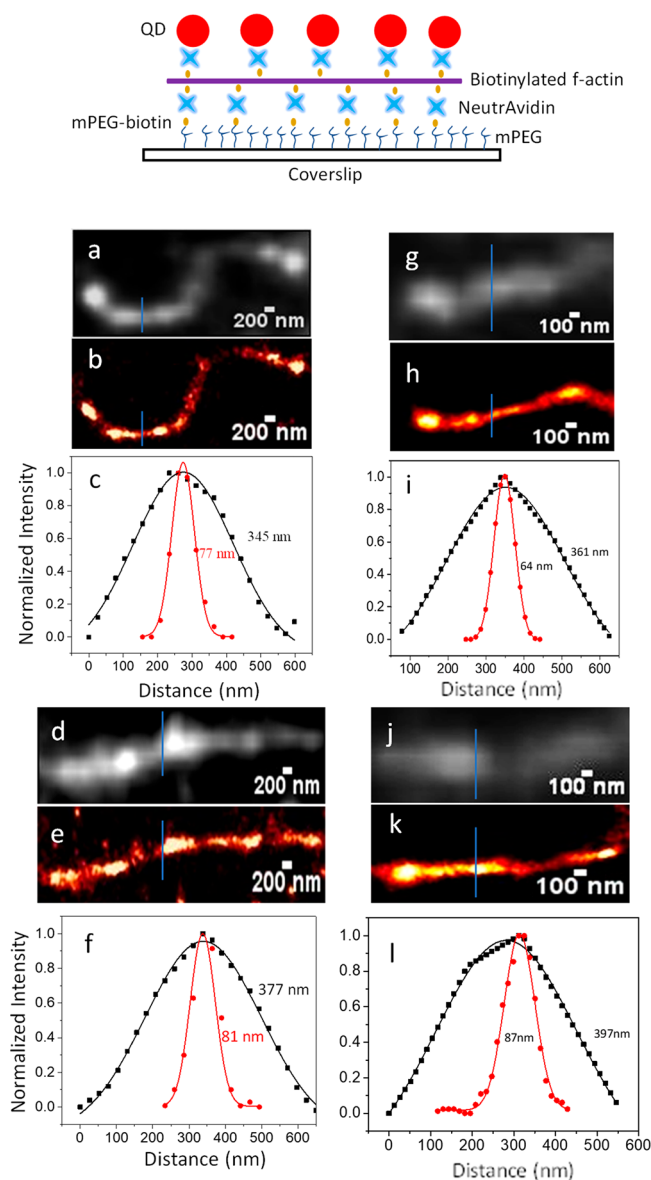


**Figure 7.** Top image shows the schematic of QD-labeled f-actin filaments. Left column of images show two examples for CIS/ZnS QDs. Right column of images show two examples for CdSe/ZnS QDs. (a, g, d, and j) Conventional TIRF images; (b, h, e, and k) reconstructed SMLM images of QD-labeled actin filaments. (c, i, f, and l) Line scan profiles (lines shown in blue in images above) of the widths of actin filaments measured using conventional TIRF imaging (black) and SMLM reconstruction (red).

The brightness of organic dyes are generally limited by their 5–20-fold lower extinction coefficient compared to QDs, so it may prove difficult to significantly improve the resolution of dye-based SMLM. Furthermore, it is still a challenge to synthesize red-emitting dyes with high PL QY and high photostability due to the extensive conjugation needed to achieve emission wavelengths above 600 nm. Thus, we believe that there is a great deal of potential for improvement of QD-based SMLM, since the optical properties of QDs can be relatively easily adjusted. For example, we have been working, and continue to work at improving the PL QY of CIS/ZnS QDs through either varying the shell thickness and composition, as we have shown to be possible for CIS/ZnS, CdSe/CdS, CdSe/ZnSe/ZnS CdSe/CdS/ZnS, or through

varying the ligands used for water-solubilization as we have shown for CdTe and CdSe/ZnS. Of course, care must be taken to not increase the total QD size too much during these modifications, and it is necessary to also maintain control of their blinking properties, or some of the advantages may be lost. As well as potential improvements in the QD fluorophores, it is also possible to improve labeling procedures to reduce nonspecific binding and/or control labeling densities. One approach may be to conjugate the QDs to actin monomers before the polymerization step rather than after it.<sup>49</sup>

## CONCLUSIONS

In summary, we have introduced compact CIS/ZnS QDs with burst-like fluorescence as probes for single molecule localization microscopy. The PL QY of CIS/ZnS QDs after phase transferring to aqueous solution is about 30% which is high enough for super resolution imaging. The average localization precision of a single QD of CIS/ZnS is 7.2 nm which is 4.5 times less precise compared to that of the brighter, commercialized CdSe/ZnS QDs. However, for super resolution imaging of actin filaments both types of QDs give comparable results for the width of actin filaments, which is about 4.5 times higher compared to those acquired from conventional TIRF imaging. Since CIS/ZnS QDs spend only ~4.2% of frames in the on state, compared to CdSe/ZnS which spend over 70% of frames in the on state, we propose that the burst-like fluorescence of CIS/ZnS QDs allows for less overlapping “ON” QDs in a given frame, which counteracts the lower brightness (and thus lower precision) of a single CIS/ZnS QD. This report highlights that CIS/ZnS QDs are a strong candidate for using compact, nontoxic QDs as excellent probes for single molecule localization imaging/super-resolution microscopy of biological structures, and further improvements to their brightness should render them even more suited for this purpose provided they can maintain their burst-like blinking.

## AUTHOR INFORMATION

### Corresponding Author

**Colin D. Heyes** – Department of Chemistry and Biochemistry, University of Arkansas, Fayetteville, Arkansas 72701, United States; [orcid.org/0000-0003-1124-9947](https://orcid.org/0000-0003-1124-9947); Email: [cheyes@uark.edu](mailto:cheyes@uark.edu)

### Authors

**Anh T. Nguyen** – Department of Chemistry and Biochemistry, University of Arkansas, Fayetteville, Arkansas 72701, United States; Present Address: Department of Chemical Engineering, Ho Chi Minh City University of Food Industry (HUF1), 140 Le Trong Tan Tay Thanh Ward Tan Phu District, Ho Chi Minh City, Viet Nam

**Dustin R. Baucom** – Department of Chemistry and Biochemistry, University of Arkansas, Fayetteville, Arkansas 72701, United States

**Yong Wang** – Department of Physics, University of Arkansas, Fayetteville, Arkansas 72701, United States; [orcid.org/0000-0002-8601-8302](https://orcid.org/0000-0002-8601-8302)

Complete contact information is available at: <https://pubs.acs.org/10.1021/cbmi.3c00018>

## Notes

The authors declare no competing financial interest.

## ACKNOWLEDGMENTS

Generous financial support by the NSF (CHE-1255440), the NIH (COBRE P30 GM103450), and the Arkansas Biosciences Institute is gratefully acknowledged. TEM instrumentation access is provided by the Arkansas Materials Characterization Facility (funded in part by the NSF) and the Institute of Nanoscience and Engineering at the University of Arkansas.

## REFERENCES

- (1) Hell, S. W. Far-field optical nanoscopy. *Science* **2007**, *316* (5828), 1153–1158.
- (2) Huang, B.; Babcock, H.; Zhuang, X. Breaking the Diffraction Barrier: Super-Resolution Imaging of Cells. *Cell* **2010**, *143* (7), 1047–1058.
- (3) Hell, S. W.; Wichmann, J. Breaking the diffraction resolution limit by stimulated emission: stimulated-emission-depletion fluorescence microscopy. *Opt. Lett.* **1994**, *19* (11), 780–782.
- (4) Klar, T. A.; Hell, S. W. Subdiffraction resolution in far-field fluorescence microscopy. *Opt. Lett.* **1999**, *24* (14), 954–956.
- (5) Gustafsson, M. G. L. Nonlinear structured-illumination microscopy: Wide-field fluorescence imaging with theoretically unlimited resolution. *Proc. Natl. Acad. Sci. U.S.A.* **2005**, *102*, 13081–13086.
- (6) Gustafsson, M. G. L. Surpassing the lateral resolution limit by a factor of two using structured illumination microscopy. *J. Microsc.* **2000**, *198*, 82–87.
- (7) Hell, S.; Stelzer, E. H. K. Properties of a 4Pi confocal fluorescence microscope. *Journal of the Optical Society of America A* **1992**, *9* (12), 2159–2166.
- (8) Hanninen, P. E.; Hell, S. W.; Salo, J.; Soini, E.; Cremer, C. Two-photon excitation 4Pi confocal microscope: enhanced axial resolution microscope for biological research. *Appl. Phys. Lett.* **1995**, *66* (13), 1698–1700.
- (9) Bewersdorf, J.; Schmidt, R.; Hell, S. W. Comparison of ISM and 4Pi-microscopy. *J. Microsc.* **2006**, *222* (2), 105–117.
- (10) Gustafsson, M.; Agard, D.; Sedat, J. Sevenfold Improvement of Axial Resolution in 3D Wide-Field Microscopy Using Two Objective-Lenses. *SPIE Proc.* **1995**, *2412* DOI: [10.1117/12.205334](https://doi.org/10.1117/12.205334).
- (11) Gustafsson; Agard; Sedat. ISM: 3D widefield light microscopy with better than 100 nm axial resolution. *J. Microsc.* **1999**, *195* (1), 10–16.
- (12) Betzig, E.; Patterson, G. H.; Sougrat, R.; Lindwasser, O. W.; Olenych, S.; Bonifacino, J. S.; Davidson, M. W.; Lippincott-Schwartz, J.; Hess, H. F. Imaging intracellular fluorescent proteins at nanometer resolution. *Science* **2006**, *313* (5793), 1642–1645.
- (13) Rust, M. J.; Bates, M.; Zhuang, X. Sub-diffraction-limit imaging by stochastic optical reconstruction microscopy (STORM). *Nat. Methods* **2006**, *3* (10), 793–795.
- (14) Sharonov, A.; Hochstrasser, R. M. Wide-field subdiffraction imaging by accumulated binding of diffusing probes. *Proc. Natl. Acad. Sci. U. S. A.* **2006**, *103* (50), 18911.
- (15) Dertinger, T.; Colyer, R.; Iyer, G.; Weiss, S.; Enderlein, J. Fast, background-free, 3D super-resolution optical fluctuation imaging (SOFI). *Proc. Natl. Acad. Sci. U.S.A.* **2009**, *106* (52), 22287–22292.
- (16) Dertinger, T.; Colyer, R.; Vogel, R.; Enderlein, J.; Weiss, S. Achieving increased resolution and more pixels with Superresolution Optical Fluctuation Imaging (SOFI). *Opt. Express* **2010**, *18* (18), 18875–18885.
- (17) Shroff, H.; Galbraith, C. G.; Galbraith, J. A.; White, H.; Gillette, J.; Olenych, S.; Davidson, M. W.; Betzig, E. Dual-color super-resolution imaging of genetically expressed probes within individual adhesion complexes. *Proc. Natl. Acad. Sci. U.S.A.* **2007**, *104* (51), 20308–20313.
- (18) Chan, W. C. W.; Nie, S. M. Quantum dot bioconjugates for ultrasensitive nonisotopic detection. *Science* **1998**, *281* (5385), 2016–2018.
- (19) Resch-Genger, U.; Grabolle, M.; Cavaliere-Jaricot, S.; Nitschke, R.; Nann, T. Quantum dots versus organic dyes as fluorescent labels. *Nat. Methods* **2008**, *5* (9), 763–775.
- (20) Lidke, K. A.; Rieger, B.; Jovin, T. M.; Heintzmann, R. Superresolution by localization of quantum dots using blinking statistics. *Opt. Express* **2005**, *13* (18), 7052–7062.
- (21) Wang, Y.; Fruhwirth, G.; Cai, E.; Ng, T.; Selvin, P. R. 3D Super-Resolution Imaging with Blinking Quantum Dots. *Nano Lett.* **2013**, *13* (11), 5233–5241.
- (22) Xu, J.; Tehrani, K. F.; Kner, P. Multicolor 3D Super-resolution Imaging by Quantum Dot Stochastic Optical Reconstruction Microscopy. *ACS Nano* **2015**, *9* (3), 2917–2925.
- (23) Chizhik, A. M.; Stein, S.; Dekaliuk, M. O.; Battle, C.; Li, W.; Huss, A.; Platen, M.; Schaap, I. A. T.; Gregor, I.; Demchenko, A. P.; Schmidt, C. F.; Enderlein, J.; Chizhik, A. I. Super-Resolution Optical Fluctuation Bio-Imaging with Dual-Color Carbon Nanodots. *Nano Lett.* **2016**, *16* (1), 237–242.
- (24) Chen, X.; Liu, Z.; Li, R.; Shan, C.; Zeng, Z.; Xue, B.; Yuan, W.; Mo, C.; Xi, P.; Wu, C.; Sun, Y. Multicolor Super-resolution Fluorescence Microscopy with Blue and Carmine Small Photo-blinking Polymer Dots. *ACS Nano* **2017**, *11* (8), 8084–8091.
- (25) Hoyer, P.; Staudt, T.; Engelhardt, J.; Hell, S. W. Quantum Dot Blueing and Blinking Enables Fluorescence Nanoscopy. *Nano Lett.* **2011**, *11* (1), 245–250.
- (26) He, H.; Liu, X.; Li, S.; Wang, X.; Wang, Q.; Li, J.; Wang, J.; Ren, H.; Ge, B.; Wang, S.; Zhang, X.; Huang, F. High-Density Super-Resolution Localization Imaging with Blinking Carbon Dots. *Anal. Chem.* **2017**, *89* (21), 11831–11838.
- (27) Zhi, B.; Cui, Y.; Wang, S.; Frank, B. P.; Williams, D. N.; Brown, R. P.; Melby, E. S.; Hamers, R. J.; Rosenzweig, Z.; Fairbrother, D. H.; Orr, G.; Haynes, C. L. Malic Acid Carbon Dots: From Super-resolution Live-Cell Imaging to Highly Efficient Separation. *ACS Nano* **2018**, *12* (6), 5741–5752.
- (28) Li, L.; Daou, T. J.; Texier, I.; Kim Chi, T. T.; Liem, N. Q.; Reiss, P. Highly Luminescent CuInS<sub>2</sub>/ZnS Core/Shell Nanocrystals: Cadmium-Free Quantum Dots for In Vivo Imaging. *Chem. Mater.* **2009**, *21* (12), 2422–2429.
- (29) Pons, T.; Pic, E.; Lequeux, N.; Cassette, E.; Bezdetsnaya, L.; Guillemain, F.; Marchal, F.; Dubertret, B. Cadmium-Free CuInS<sub>2</sub>/ZnS Quantum Dots for Sentinel Lymph Node Imaging with Reduced Toxicity. *ACS Nano* **2010**, *4* (5), 2531–2538.
- (30) Mandal, G.; Darragh, M.; Wang, Y. A.; Heyes, C. D. Cadmium-free quantum dots as time-gated bioimaging probes in highly-autofluorescent human breast cancer cells. *Chem. Commun.* **2013**, *49* (6), 624–626.
- (31) Ding, K.; Jing, L.; Liu, C.; Hou, Y.; Gao, M. Magnetically engineered Cd-free quantum dots as dual-modality probes for fluorescence/magnetic resonance imaging of tumors. *Biomaterials* **2014**, *35* (5), 1608–1617.
- (32) Jiao, M.; Huang, X.; Ma, L.; Li, Y.; Zhang, P.; Wei, X.; Jing, L.; Luo, X.; Rogach, A. L.; Gao, M. Biocompatible off-stoichiometric copper indium sulfide quantum dots with tunable near-infrared emission via aqueous based synthesis. *Chem. Commun.* **2019**, *55* (100), 15053–15056.
- (33) Nguyen, A. T.; Gao, F.; Baucom, D.; Heyes, C. D. CuInS<sub>2</sub>-Doped ZnS Quantum Dots Obtained via Non-Injection Cation Exchange Show Reduced but Heterogeneous Blinking and Provide Insights into Their Structure-Optical Property Relationships. *J. Phys. Chem. C* **2020**, *124* (19), 10744–10754.
- (34) Li, L.; Pandey, A.; Werder, D. J.; Khanal, B. P.; Pietryga, J. M.; Klimov, V. I. Efficient Synthesis of Highly Luminescent Copper Indium Sulfide-Based Core/Shell Nanocrystals with Surprisingly Long-Lived Emission. *J. Am. Chem. Soc.* **2011**, *133* (5), 1176–1179.
- (35) Ovesný, M.; Křížek, P.; Borkovec, J.; Švindrych, Z.; Hagen, G. M. ThunderSTORM: a comprehensive ImageJ plug-in for PALM and

STORM data analysis and super-resolution imaging. *Bioinformatics* **2014**, *30* (16), 2389–2390 (accessed 4/15/2020).

(36) Cai, E.; Ge, P.; Lee, S. H.; Jeyifous, O.; Wang, Y.; Liu, Y.; Wilson, K. M.; Lim, S. J.; Baird, M. A.; Stone, J. E.; Lee, K. Y.; Davidson, M. W.; Chung, H. J.; Schulten, K.; Smith, A. M.; Green, W. N.; Selvin, P. R. Stable Small Quantum Dots for Synaptic Receptor Tracking on Live Neurons. *Angew. Chem., Int. Ed.* **2014**, *53* (46), 12484–12488.

(37) Zhao, C.; Bai, Z.; Liu, X.; Zhang, Y.; Zou, B.; Zhong, H. Small GSH-Capped CuInS<sub>2</sub> Quantum Dots: MPA-Assisted Aqueous Phase Transfer and Bioimaging Applications. *ACS Appl. Mater. Interfaces* **2015**, *7* (32), 17623–17629.

(38) Breus, V. V.; Heyes, C. D.; Nienhaus, G. U. Quenching of CdSe-ZnS core-shell quantum dot luminescence by water-soluble thiolated ligands. *J. Phys. Chem. C* **2007**, *111* (50), 18589–18594.

(39) Luan, W.; Yang, H.; Wan, Z.; Yuan, B.; Yu, X.; Tu, S.-t. Mercaptopropionic acid capped CdSe/ZnS quantum dots as fluorescence probe for lead(II). *J. Nanopart. Res.* **2012**, *14* (3), 762.

(40) Nirmal, M.; Dabbousi, B. O.; Bawendi, M. G.; Macklin, J. J.; Trautman, J. K.; Harris, T. D.; Brus, L. E. Fluorescence intermittency in single cadmium selenide nanocrystals. *Nature* **1996**, *383* (6603), 802–804.

(41) Heyes, C. D. Chapter 4—Quantum dots in single molecule spectroscopy. In *Spectroscopy and Dynamics of Single Molecules*; Johnson, C. K., Ed.; Elsevier: Amsterdam, 2019; pp 163–228.

(42) Galland, C.; Ghosh, Y.; Steinbrück, A.; Sykora, M.; Hollingsworth, J. A.; Klimov, V. I.; Htoon, H. Two types of luminescence blinking revealed by spectroelectrochemistry of single quantum dots. *Nature* **2011**, *479* (7372), 203–207.

(43) Schmidt, R.; Krasselt, C.; Gohler, C.; von Borczyskowski, C. The Fluorescence Intermittency for Quantum Dots Is Not Power-Law Distributed: A Luminescence Intensity Resolved Approach. *ACS Nano* **2014**, *8* (4), 3506–3521.

(44) Bajwa, P.; Gao, F.; Nguyen, A.; Omogo, B.; Heyes, C. D. Influence of the Inner-Shell Architecture on Quantum Yield and Blinking Dynamics in Core/Multishell Quantum Dots. *ChemPhysChem* **2016**, *17* (5), 731–740.

(45) Durisic, N.; Godin, A. G.; Walters, D.; Grutter, P.; Wiseman, P. W.; Heyes, C. D. Probing the “Dark” Fraction of Core-Shell Quantum Dots by Ensemble and Single Particle pH-Dependent Spectroscopy. *ACS Nano* **2011**, *5* (11), 9062–9073.

(46) Durisic, N.; Wiseman, P. W.; Grutter, P.; Heyes, C. D. A Common Mechanism Underlies the Dark Fraction Formation and Fluorescence Blinking of Quantum Dots. *ACS Nano* **2009**, *3* (5), 1167–1175.

(47) Whitham, P. J.; Marchioro, A.; Knowles, K. E.; Kilburn, T. B.; Reid, P. J.; Gamelin, D. R. Single-Particle Photoluminescence Spectra, Blinking, and Delayed Luminescence of Colloidal CuInS<sub>2</sub> Nanocrystals. *J. Phys. Chem. C* **2016**, *120* (30), 17136–17142.

(48) Thompson, R. E.; Larson, D. R.; Webb, W. W. Precise nanometer localization analysis for individual fluorescent probes. *Biophys. J.* **2002**, *82* (5), 2775–2783.

(49) Patolsky, F.; Weizmann, Y.; Willner, I. Actin-based metallic nanowires as bio-nanotransporters. *Nat. Mater.* **2004**, *3* (10), 692–695.

(50) Wu, K. C.-W.; Yang, C.-Y.; Cheng, C.-M. Using cell structures to develop functional nanomaterials and nanostructures - case studies of actin filaments and microtubules. *Chem. Commun.* **2014**, *50* (32), 4148–4157.

(51) Xu, K.; Babcock, H. P.; Zhuang, X. Dual-objective STORM reveals three-dimensional filament organization in the actin cytoskeleton. *Nat. Methods* **2012**, *9* (2), 185–188.

(52) Izeddin, I.; El Beheiry, M.; Andilla, J.; Ciepielewski, D.; Darzacq, X.; Dahan, M. PSF shaping using adaptive optics for three-dimensional single-molecule super-resolution imaging and tracking. *Opt. Express* **2012**, *20* (5), 4957–4967.

(53) van de Linde, S.; Wolter, S.; Heilemann, M.; Sauer, M. The effect of photoswitching kinetics and labeling densities on super-

resolution fluorescence imaging. *J. Biotechnol.* **2010**, *149* (4), 260–266.